Minimal realisations of OMA-based FIs: The proposed circuits are shown in Fig. 2 and like the circuits of [1], realise an FI of value $Z_{1\text{-}2} = Z_1Z_2/Z_3$ without requiring any passive component matching conditions. Changing the connections a_1–b_1, a_2–b_2 to a_1–b_2, a_2–b_1 facilitates the realisation of negative FIs from the same circuits. A variety of single-resistance-tunable floating elements (such as ideal floating inductance, ideal resistively-variable floating capacitance, ideal floating FDNR etc.) are realisable by appropriate choice (resistive/capacitive) of impedances Z_1, Z_2 and Z_3. Thus, the structures proposed here possess all the properties of their predecessors [1] (quoted above), while requiring only three OMA(–)s as opposed to four OMA(–)s in the structures of [1].

From the considerations of [14–16], it follows that the FI configurations of the intended type (i.e. various kinds of FIs in lossless forms, without requiring any component matching and using only three passive components) cannot be realised with less than three nullors (OFA/OMA(–)). Consequently, the new circuits of Fig. 2 are minimal in that they require not only a minimum number of passive components but also a minimum number of OMAs.

Hardware reduction: It is interesting to note that in the structures of Fig. 2, OMA(–)s A_1 and A_2 can be replaced by OMA(+)s without affecting the realised FI value. This results in a saving (see note 1) of four CMs over the entirely OMA(–) based versions requiring 12 CMs.

Comparison with previously published CC-based FIs: In the structures discussed here, OMA(–) and OMA(+) are essentially configured as current conveyors (CCs) (CCII– and CCII+, respectively), and therefore the proposed configuration can also be implemented by integrated CCs, many varieties of which are now commercially available such as PA630 [4], AD844 [5] and LTP CCII01 [6]. On studying the three-CC-based FI simulation networks already published in earlier literature [7–13] we observed that out of the circuits of Fig. 2*a–d*, only the CC version of the circuit of Fig. 2*c* was known previously [10]; the remainder are all believed to be completely new. Moreover, the feasibility of realising positive as well as negative FIs from the same circuits is not mentioned in the earlier works [7–13].

Conclusion: Although additional circuits of the type presented here are possible employing the opamps inside the OMAs configured in infinite gain mode (note that in such cases OMAs would no longer be equivalent to CCs) by invoking various network transformations following the methodology of [1], we have presented here only those structures in which the opamps in the OMAs are connected as unity gain amplifiers because such structures are generally found to be superior to other alternatives from the point of view of practical considerations of stability and operational frequency range.

Acknowledgment: This paper is partly based on work carried out by the authors into the 'synthesis of floating immittance structures using OMAs' at the Linear Integrated Circuits Lab. of Delhi Institute of Technology, during the period May 1992–June 1993.

11 May 1994
Electronics Letters Online No: 19940791

R. Senani (*Department of Electronics and Communication Engineering, Delhi Institute of Technology, Old I. G. Block, Kashmere Gate, Delhi 110006, India*)

J. Malhotra (*130, Basant Enclave (S.F.S. Flats), New Delhi 110057, India*)

References

1 MALHOTRA, J., and SENANI, R.: 'Class of floating generalised positive/negative immitance converters/inverters realised with operational mirrored amplifiers', *Electron. Lett.*, 1994, **30**, (1), pp. 3–5

2 WILSON, B.: 'Recent developments in current conveyors and current mode circuits', *IEE Proc. G.*, 1990, **137**, (2), pp. 63–77

3 NORMAND, G.: 'Floating impedance realisation using a dual operational mirrored amplifier', *Electron. Lett.*, 1986, **22**, (10), pp. 521–522

4 WADSWORTH, D.C.: 'Accurate current conveyor topology and monolithic implementation', *IEE Proc. G.*, 1990, **137**, (2), pp. 88–94

5 SVOBODA, J.A., MCGORY, L., and WEBB, S.: 'Applications of a commercially available current conveyor', *Int. J. Electron.*, 1990, **70**, pp. 159–164

6 TOUMAZOU, C., PAYNE, A., and LIDGEY, J.: 'Current feedback versus feedback amplifiers: History, insight and relationships'. Proc. Int. Symp. Circuits and Systems, 1993, (Chicago, Illinois), pp. 1046–1049

7 SENANI, R.: 'New tunable synthetic floating inductors', *Electron. Lett.*, 1980, **16**, (10), pp. 382–383

8 NANDI, S., JANA, P.B., and NANDI, R.: 'Floating ideal FDNR using current conveyors', *Electron. Lett.*, 1983, **19**, (7), pp. 251–

9 NANDI, S., JANA, P.B., and NANDI, R.: 'Novel floating ideal tunable FDNR simulation using current conveyors', *IEEE Trans.*, 1984, **CAS-31**, (4), pp. 402–403

10 ABDALLA, Y.A.N.: 'Comments on 'Novel floating tunable FDNR simulation using current conveyors'', *IEEE Trans.*, 1985, **32**, (3), pp. 303–

11 HIGASHIMURA, M., and FUKUI, Y.: 'Novel lossless tunable FDNR simulation using two current conveyors and a buffer', *Electron. Lett.*, 1986, **22**, (18), pp. 938–939

12 HIGASHIMURA, M., and FUKUI, Y.: 'Realisation of floating immitance using three current conveyors', *IECE Trans. Jpn.*, 1987, **J70-A**, pp. 1203–1204

13 HIGASHIMURA, M., and FUKUI, Y.: 'New lossless tunable FDNR simulation using two current conveyors and an INIC', *Electron. Lett.*, 1987, **23**, (10), pp. 498–499

14 DEPRETTERE, E.: 'On the minimal realisation of the gyrator by means of nullors and resistors - Part I', *Int. J. Circuit Theory and Applications*, 1975, **3**, pp. 383–390

15 DEPRETTERE, E.: 'On the minimal realisation of the gyrator by means of nullors and resistors - Part II', *Int. J. Circuit Theory and Applications*, 1976, **4**, pp. 285–297

16 SILVA, M.M.: 'On the realisation of immittance inverters with a minimum number of active components', *IEEE Trans.*, 1979, **CAS-26**, (11), pp. 931–935

17 TOUMAZOU, C., LIDGEY, F.J., and HAIGH, D.G.: 'Analog IC design: The current mode approach' (Peter Peregrinus Ltd., 1990), Chap. 4, pp. 150–153

Note 1. A study of the structures of [1] shows that they can also be implemented with four OMA(+)s rather than four OMA(–)s. With such a change, the OMA(+) version of one of the eight structures therein fig. 2*a* of [1] becomes quite similar to the Toumazou and Lidgey (see [17]).

Adaptive importance sampling for fading channels

W. Zhuang

Indexing terms: Fading, Mobile radio systems, Monte Carlo methods

The authors present an adaptive importance sampling (AIS) technique for estimating the bit error rate of a digital communications system over a correlated Rayleigh fading channel. The technique reduces the computer simulation time significantly and simplifies the procedure of choosing an optimally-biased density function of the channel fading process.

Introduction: Computer simulation is an essential tool for accessing the bit error rate (BER) performance of a digital communications system. Over a correlated fading channel, the confidence interval of the BER estimate depends not only on the number of error events but also on the number of fading cycles which the system experienced. In the case of high received signal-to-noise (SNR) ratio, the number of fading cycles is a dominant factor. For a very slowly fading channel, each fading cycle corresponds to a large number of transmitted data bits, only a very small portion of which will result in error events. Therefore, importance sampling (IS) techniques are necessary to reduce computer simulation time. The trial and error method and others are often used to select the biased probability densities, which are far from optimal.

Recently adaptive importance sampling (AIS) has been investigated for BER estimation over an additive white Gaussian noise (AWGN) channel [1]. This Letter presents an AIS technique for a Rayleigh fading channel. An adaptive algorithm is given that can be used to search for optimally biased probability densities during the course of IS simulation. The AIS technique iteratively adapts the biased probability densities to be optimal, and considerably reduces the computer simulation time.

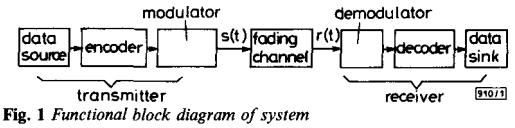

Fig. 1 *Functional block diagram of system*

System description and importance sampling: A simplified system functional block diagram is shown in Fig. 1. The fading channel corrupts the signalling waveform $s(t)$ by introducing a Rayleigh distributed multiplicative envelope distortion $\gamma(t)$ and a carrier phase disturbance $\psi(t)$ uniformly distributed over $[0, 2\pi]$. The received signal $r(t)$ is also degraded by AWGN $n(t)$. The system BER performance depends on $s(t)$, $\gamma(t)e^{-j\psi(t)}$ and $n(t)$. The PDF of $\gamma(t)$ is

$$f_\gamma(\gamma) = \begin{cases} (\gamma/\sigma_\gamma^2)\exp(-\gamma^2/2\sigma_\gamma^2) & \gamma \geq 0 \\ 0 & \gamma < 0 \end{cases} \quad (1)$$

If the same form of the PDF is desired, then the weighting function $w(\gamma)$ with a modified parameter σ_γ^* is

$$w(\gamma) = \frac{f_\gamma(\gamma)}{f_\gamma^*(\gamma)} = \frac{\sigma_\gamma^{*2}}{\sigma_\gamma^2}\exp\left[\frac{\gamma^2(\sigma_\gamma^2 - \sigma_\gamma^{*2})}{2\sigma_\gamma^2\sigma_\gamma^{*2}}\right] \quad \gamma \geq 0 \quad (2)$$

With IS, the simulation process for each BER value is divided into a number of short sub-simulations. The fading process Γ^* is correlated according to eqn. 1.3-7 in [2] in each sub-simulation, but uncorrelated for different sub-simulations. As a result, the system can go through all the statistical statuses of the channel fading in a shorter period compared with that of a single long simulation. Each sub-simulation is long enough to take into account the system memory, so that the BER estimate is not affected by the simulation division. The optimally biased variance σ_γ^{*2} is the value which minimises the variance of the estimation error (σ_e^2). Because σ_e^2 is a function of p_e to be estimated, the optimal σ_γ^{*2} cannot be obtained directly by minimising σ_e^2. In the following, an adaptive recursive algorithm is presented to obtain the optimal σ_γ^{*2} during the course of simulation.

Adaptive algorithm for weighting function: During each sub-simulation, p_e is estimated; when error events occur, the samples of the channel fading are noted, which are distributed according to the unknown optimal IS density. These fading samples are used to estimate the optimal σ_γ^{*2} which is then used to generate channel fading samples for the next sub-simulation. With AIS the estimation of the optimal weighting function is performed at the same time as the estimation of p_e, and is then used in the next sub-simulation. From eqn. 1,

$$E\{\gamma^2\} = \int_{-\infty}^{\infty} \gamma^2 f_\gamma(\gamma)d\gamma = 2\sigma_\gamma^2 \quad (3)$$

therefore, an estimate of the biased σ_γ^{*2} can be obtained from the expectation of the fading samples which cause error events, which is

$$\mu = E(\gamma^2|\gamma \in \Xi) = \int_\Xi \gamma^2 \frac{f_\gamma(\gamma)}{p_e}d\gamma = \frac{p_e^*}{p_e}\bar{\gamma}^2 \quad (4)$$

where Ξ is the set of γ which corresponds to an error event, p_e^* is the probability of error and $\bar{\gamma}^2 = E^*[\gamma^2 w(\gamma)|\gamma \in \Xi]$ is the mean when $f^*(\gamma)$ is used. Because the white Gaussian noise samples are i.i.d. random variables, and the channel fading samples are correlated in each sub-simulation, the adaptive algorithms [1] developed for the optimal biased PDF of the Gaussian noise are not directly applicable to correlated channel fading. Only the independent samples should be used for estimating $\bar{\gamma}^2$ in order to reduce the variance of the estimation error, which may be a very small number in each sub-simulation. To increase the size of the independent samples, all the independent fading samples causing error events in the previous sub-simulations should be used to bias the IS density for the next sub-simulation. A new recursive algorithm is given here to estimate $\bar{\gamma}^2$:

$$\bar{\gamma}_0^2 = \frac{1}{p_0}\sum_{k=1}^{p_0}\gamma_{0k}^2 w_0(\gamma_{0k}) \quad m_0 = p_0 \quad (5)$$

$$\bar{\gamma}_i^2 = \frac{m_{i-1}}{m_i}\bar{\gamma}_{i-1}^2 + \frac{1}{m_i}\sum_{k=1}^{p_i}\gamma_{ik}^2 w_i(\gamma_{ik}) \quad m_i = m_{i-1} + p_i \quad (6)$$

where p_i and m_i are the numbers of independent samples in the ith sub-simulation, and up to the ith sub-simulation, respectively, γ_{ik} is the kth independent sample in the ith sub-simulation, all these fading samples causing error events; $w_i(\cdot)$ is the weighting density of the ith sub-simulation. The estimate of μ after the Ith sub-simulation can be derived as

$$\hat{\mu}_I = \bar{\gamma}_I^2/[(1/m_I)\sum_{i=1}^{I}\sum_{k=1}^{p_i} w_i(\gamma_{ik})] \quad (7)$$

which is a weakly consistent estimator of μ. The updated biased density function $f_\gamma^*(\gamma)$ for the next sub-simulation is achieved with $\hat{\sigma}_\gamma^{*2} = (1/2)\hat{\mu}_I$.

Table 1: Sample size and improvement ratio

SNR/bit	Sample size			Improvement ratio	
	MC	IS	AIS	IS	AIS
dB					
10	5.0×10^5	1.0×10^4	3.0×10^3	50	167
15	5.0×10^5	1.0×10^4	3.0×10^3	50	167
20	5.0×10^5	1.0×10^4	3.0×10^3	50	167
25	5.0×10^5	1.0×10^4	3.0×10^3	50	167
30	5.0×10^5	1.0×10^4	3.0×10^3	50	167
35	5.0×10^5	1.0×10^4	3.0×10^3	50	167
40	1.0×10^6	1.2×10^4	3.0×10^3	83	333
45	1.5×10^6	1.4×10^4	3.0×10^3	107	500

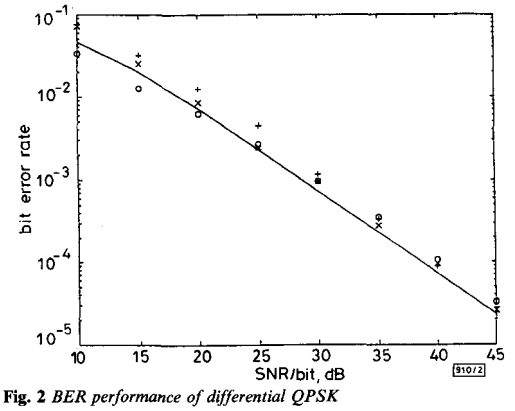

Fig. 2 *BER performance of differential QPSK*

— theoretical analysis
\+ MC simulation
o IS simulation
× AIS simulation

Example: Differential QPSK: Fig. 2 shows the BER performance of differential QPSK based on theoretical analysis, Monte Carlo (MC) simulation, IS simulation (with a biased PDF of the channel fading process with $\sigma_\gamma^{*2} = 0.1\sigma_\gamma^2$ obtained by trial and error), and AIS simulation. A channel fading rate of 10^{-4} is selected. Fig. 3 shows the convergence of the estimated optimal σ_γ^{*2} for the (SNR/bit) values ranging from 10dB to 45dB. Table 1 gives the data sample size and the improvement ratio of the computer simulations. The sample sizes are necessary for achieving the BER estimates with a 90% confidence interval of ($BER = 0.5$, $BER = 2.0$).

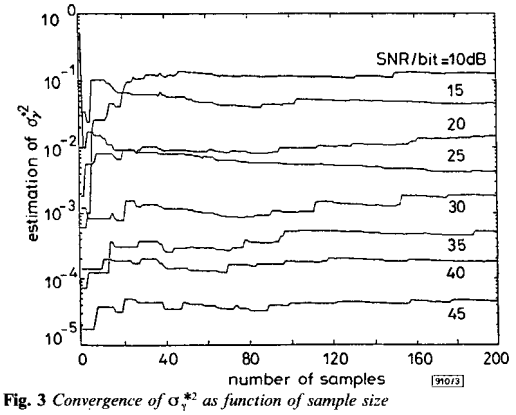

Fig. 3 *Convergence of σ_Y^{*2} as function of sample size*

The IS simulation reduces the data sample sizes by at least 50 times compared with those of MC simulations, however it is burdened by the necessity of choosing correct σ_Y^{*2} values. The AIS further reduces both data sample size by at least 167 times and computer time for searching the optimal densities. The improvement ratio increases as the value of (SNR/bit) increases. The advantage of AIS simulation over simple IS simulation is clearly observed from the simulation results.

25 April 1994
Electronics Letters Online No: 19940786

W. Zhuang (*Dept. of Elec. & Comp. Eng., University of Waterloo, Waterloo, Ontario, N2L 3G1, Canada*)

References

1 STADLER, J.S., and ROY, S.: 'Adaptive importance sampling', *IEEE J. Sel. Areas Commun.*, April 1993, **SAC-11**, pp. 309–316
2 JAKES, W.C.: 'Microwave mobile communications' (Wiley, New York, 1974)

Exact fluid-flow analysis of single on/off source feeding an ATM buffer

J. Schormans, J. Pitts and L. Cuthbert

Indexing terms: Asynchronous transfer mode, Queueing theory

A formula is developed to calculate the cell loss probability for an ATM buffer fed by a single ON/OFF source. This fluid-flow method uses balance equations to give a geometric progression for the state probabilities. Results show better accuracy than fluid-flow analysis based on differential equations. This cell loss formula can be applied as a more accurate component in connection admission control and bandwidth management algorithms for ATM networks.

Introduction: The analysis of a single on/off source feeding a finite queue with a deterministic server is an essential component in the design of connection admission control (CAC) algorithms based on the concept of equivalent capacity [1]. This concept defines a bandwidth value, between the mean and peak rates of a variable bit-rate source, as the amount to be allocated to satisfy performance requirements such as the maximum permitted cell loss probability. The key feature of this analysis is that it deals fundamentally with rates. When the source rate exceeds the queue's service rate, the queue begins to fill and ultimately, for a finite queue, it overflows. This is called burst-scale congestion [2].

In the literature, this is analysed using fluid-flow techniques based on those of Anick *et al.* [3] and Tucker [4] but for a single source rather than multiple sources (see [1,5]). Such analysis is recognised as an approximation to the actual queueing operation because cell-scale congestion is not modelled [2,4]. However, there is another approximation inherent in this model: cells are discrete units which do not exist in fractional quantities, and this does make a difference to the actual queue operation and to the cell loss results.

In this Letter we use a rate based model, analogous to standard fluid-flow analysis, but one which considers changes to the queue size in discrete steps rather than approximating them as continuously variable. This was achieved by using balance equations, rather than with partial differential equations which treat the queue size as a continuum. A key feature of this approach is its mathematical elegance; the state probabilities were found to be a geometric progression giving a closed form solution for the cell loss probability. Results comparing both analytical approaches with cell-scale analysis (in the limited case where this is possible) clearly show the accuracy of our method.

The design of CAC algorithms is a tradeoff between methods that are simple and fast but inaccurate, and those that are complicated and slow but accurate. This analysis supplies, for bandwidth management schemes based on the concept of equivalent capacity, a fundamental component that combines the best of both: it is simple, fast and accurate.

System model: The analysis considers queueing at the 'burst level'. We define R to be the actual cell arrival rate, C the actual cell transmission rate, $E[ON\ time]$ the expected on time for the source, and $E[OFF\ time]$ the expected off time for the source. If the source is in the OFF state and the buffer is empty, then it remains empty; if the buffer is not empty, then it empties at a constant rate C. If the source is in the ON state and the buffer is not full, then it fills at a constant rate R–C; if the buffer is full, then cells are lost at a constant rate R–C.

As is normal with such source models, we assume that the sojourn time in each state is memoryless; the OFF period lasts for a geometrically distributed number of timeslots and the ON period lasts for a geometrically distributed number of 'burst-level' arrivals (i.e. where the arrival rate is considered to be the excess rate R–C).

Once the source has entered the OFF state, it will stay there for at least one time slot; after each time slot in the OFF state the source remains in the OFF state with a probability 's'. Once the source has entered the ON state, it will generate at least one 'excess-rate' arrival. After each one of these arrivals the source generates another 'excess-rate' arrival with a probability 'a'. Because the ON and OFF periods are geometrically distributed, we have

$$E[\text{number of 'excess-rate' arrivals in an ON period}] = 1/(1-a)$$

$$E[\text{number of time slots in an OFF period}] = 1/(1-s)$$

Now

$$E[\text{number of 'excess-rate' arrivals in an ON period}] = E[\text{ON time}](R-C)$$

so

$$a = 1-1/(E[\text{ON time}](R-C))$$

Also

$$E[\text{number of time slots in an OFF period}] = E[\text{OFF time}]C$$

so

$$s = 1-1/(E[\text{OFF time}]C)$$

Queueing analysis: We define N as the buffer capacity, CLP as the exact cell loss probability and $p[k] = p[$an 'excess-rate' cell finds k cells in the queue on arrival$]$. For the level between states N–1 and N, equating probabilities gives

$$a.p[N-1] = p[N](1-a)$$

where the left hand side is the probability of crossing up (i.e. arrival i sees N–1, arrival i+1 sees N) and the right hand side is the probability of crossing down (i.e. arrival i sees N and is lost, arrival i+1 sees N–1 or fewer). Therefore

$$a.p[N-1] = p[N](1-a)$$